https://doi.org/10.5194/essd-2025-694
Preprint. Discussion started: 3 December 2025

Open Access Earth System Science Data Discussions

A global gridded dataset of significant wave height via fusion of multi-mission altimetry and numerical hindcast

Haoyu Jiang [1,2,3*] , Hao Su [3]

[1]College of Life Sciences and Oceanography, Shenzhen University, Shenzhen 518000, China
[2]Laboratory for Regional Oceanography and Numerical Modeling, Qingdao Marine Science and Technology Center, Qingdao 266000, China
[3]Shenzhen Research Institute, China University of Geosciences, Shenzhen 518000, China

Correspondence to: Haoyu Jiang (Haoyujiang@szu.edu.cn)

Abstract. Satellite altimeters provide long-term, high-accuracy observations of significant wave height (SWH) over the global ocean. However, their sparse spatial and temporal sampling introduces undersampling errors in wave climate analyses. Direct gridding of multi-mission altimeter data through spatiotemporal interpolation still results in low-accuracy global SWH fields due to this limitation. To overcome this challenge, we use SWH outputs from a WAVEWATCH III hindcast as a background field and apply an offline post-fusion with along-track, jointly calibrated altimeter observations from the Climate Change Initiative Sea State dataset. Unlike data assimilation within numerical wave models, this offline fusion approach allows retrospective correction of past model outputs using future observations. Validation against buoy measurements and independent satellite data demonstrates that the fused gridded product achieves high accuracy. To address different application needs, we provide two versions of the fused dataset: 1) A “two-sat” version that incorporates data from only two satellites at any given time, designed for wave climate studies. This configuration ensures temporal consistency by maintaining a stable data volume over the entire time span. 2) A “multi-sat” version that integrates data from as many altimeter missions as possible, intended to support applications such as the training of artificial intelligence-based wave models, where higher spatial and temporal accuracy is prioritized. The dataset is freely available at https://doi.org/10.57760/sciencedb.29314 (Su and Jiang, 2025).

1 Introduction

Wind-generated surface gravity waves (hereafter referred to as waves) are a ubiquitous oceanic phenomenon and play a crucial role in air–sea interactions. A statistical understanding of wave behaviour, commonly referred to as the wave climate, and its variability under changing climate conditions is vital from both scientific and societal perspectives (e.g., ocean engineering, coastal protection, marine renewable energy, and climate assessment). As a result, wave climate has been extensively studied over the past two decades.

https://doi.org/10.5194/essd-2025-694
Preprint. Discussion started: 3 December 2025

To investigate historical wave climate and its variability, long-term wave datasets are essential. Currently, three primary sources of wave data are commonly used in wave climate studies: in situ observations, satellite remote sensing, and Numerical Wave Models (NWMs), each with its own strengths and limitations. Among them, in situ wave buoys with long-term records are very limited in number and are predominantly located along the coastlines of developed countries. This sparse and uneven spatial distribution makes them unsuitable for large-scale wave climate analyses.

Satellite remote sensing, particularly satellite altimetry, provides high-accuracy measurements of global Significant Wave Height (SWH) and has accumulated over 30 years of observations (e.g., Zieger et al., 2009; Ribal and Young, 2019; Dodet et al., 2020). Systematic inter-calibrations of multiple past and present altimeter missions have been conducted by Ribal and Young (2019) and Dodet et al. (2020), resulting in consistent multi-mission SWH datasets spanning more than three decades. These datasets have enabled comprehensive investigations of long-term global wave climate variability (e.g., Young and Ribal, 2020; Timmermans et al., 2020).

However, altimeters, as well as other satellite-based wave sensors such as the wave model of synthetic aperture radar and wave scatterometers, are narrow with respect to swath widths, leading to sparse spatiotemporal sampling. Altimeters typically have an across-track spacing of 300–500 km and revisit periods of 10 days or more. This sparse sampling often fails to capture rapidly evolving sea states or extreme events, introducing significant undersampling errors in wave climate analyses, particularly in the estimation of high percentiles (e.g., 90th and 99th) and their trends. Such errors may lead to misleading conclusions (Jiang, 2020).

To support robust wave climate studies, a long-term, accurate, and seamless (gridded) wave dataset is essential. NWMs have been widely used to reconstruct historical global wave climate by forcing the models with historical wind fields (e.g., Sterl and Caires, 2005; Semedo et al., 2011, 2015; Fan et al., 2012; Stopa et al., 2014; Meucci et al., 2018). When forced with projected wind fields from climate models, NWMs can also be used to estimate future wave conditions (e.g., Fan et al., 2013, 2014; Semedo et al., 2013). However, NWMs are subject to both physical and numerical limitations. While they can reproduce the general patterns of wave height distributions, their ability to accurately simulate extreme wave events remains a subject of debate. In addition, the wind hindcasts used to drive NWMs often suffer from temporal inhomogeneities due to changes in the amount and quality of assimilated atmospheric observations over time, potentially introducing non-climatic artifacts into the wave hindcast data.

Another type of gridded wave dataset is the Level-4 product derived from multi-mission altimeter measurements through spatiotemporal interpolation, such as the *Global Ocean L4 SWH from NRT Satellite Measurements* (CMEMS, 2024, https://doi.org/10.48670/moi-00180). However, due to the severe undersampling inherent to satellite altimetry and the high spatiotemporal variability of ocean waves, such interpolation-based products still suffer from significant limitations. Specifically, they typically have coarse spatial and temporal resolutions (e.g., 2° × 2° × 1 day). More importantly, the accuracy of these “independent” Level-4 products is often markedly lower than that of the original along-track observations, and in many cases, even lower than that of NWM outputs (see Section 3 for related results).

https://doi.org/10.5194/essd-2025-694
Preprint. Discussion started: 3 December 2025

A more promising approach for generating high-quality SWH dataset is to combine the seamless spatiotemporal coverage of NWM hindcasts with the higher accuracy of satellite altimeter observations. Such fusion or assimilation strategies aim to leverage the strengths of both data sources. One widely used example is the ERA5 wave reanalysis dataset (Hersbach et al., 2020), which is part of the ERA5 climate reanalysis covering the period from 1950 to the present. It provide hourly data many wave parameters, including SWH, with a resolution 0.5°×0.5°×1h. In the ERA5 wave model, SWH observations from multiple altimeter missions, including ERS-1/2, ENVISAT, JASON-1/2, CRYOSAT-2, and SARAL, are assimilated using a spatial optimal interpolation method. This assimilation reduces errors in the NWM hindcast to some extent. However, the "online" assimilation methodology in ERA5 presents several limitations when used for historical SWH data reconstruction:

1) Lack of jointly calibration: The altimeter SWH data used in ERA5 are not jointly calibrated across missions. Instead, observations from individual satellites are first regressed to match the model hindcast baseline before assimilation. While this helps mitigate inter-mission biases, it may also suppress real climate signals contained in the altimeter data due to biases in the model background.

2) Forward-only assimilation: The assimilation scheme in ERA5 considers only past and current SWH observations to constrain the future wave state. Due to the absence of a backward model (which is challenging for NWMs because the alleviation of the garden sprinkler effect is difficult to reverse), the assimilation scheme does not account for the influence of future altimeter SWH observations on past wave states, thereby limiting the extent to which observational data can be fully utilized in reconstructing historical wave fields.

3）Uncertainty in spectral corrections: In "online" assimilation of NWMs, adjustments must be made to the shape of the directional wave spectra after the correction of SWH. Several approaches exist for correcting spectral shapes from SWH alone, but these methods can introduce additional uncertainty. In some cases, improper spectral corrections may even degrade the overall accuracy of the assimilated results.

To address the limitations outlined above, this study presents a dataset that fuses jointly calibrated satellite altimeter observations with NWM hindcast outputs. This dataset effectively mitigates the undersampling issue inherent to altimetry while preserving the wave variability signals captured by the altimeters, making it well suited for wave climate studies. In addition, the rapid advancement of deep learning techniques has led to growing interest in data-driven wave modeling. These models typically require seamless and reliable datasets as "truth" for training. Therefore, beyond its value for wave climate analysis, the fused dataset introduced in this study also provides a valuable resource for a wide range of applications, including the development of deep learning-based wave models and SWH post-correction models.

This paper describes the production methodology, validation, and access information for the fused dataset. Section 2 introduces the jointly calibrated altimeter observations and NWM hindcasts used as inputs, along with the reference datasets employed for validation and comparison, including buoy measurements and a Level-4 gridded SWH product. Section 3 details the processing steps for generating the fused dataset. Section 4 presents its evaluation results, followed by discussions in Section 5.

https://doi.org/10.5194/essd-2025-694
Preprint. Discussion started: 3 December 2025

2 Data and Methods

2.1 Data

2.1.1 CCI-Sea State Dataset

The most important altimeter dataset used in this study is the Level-3 1-Hz significant wave height (SWH) product from the CCI (Climate Change Initiative) Sea State dataset (Dodet et al., 2020). The CCI-Sea State project, developed by the European Space Agency, aims to provide a long-term and consistent satellite-based record of sea state. This dataset integrates observations from multiple radar altimeter missions, including ERS-1/2, TOPEX, JASON-1/2/3, ENVISAT, CRYOSAT-2, SARAL, and Sentinel-3A/3B/6. Rigorous quality control, cross-calibration, and denoising procedures are applied to enhance the accuracy and consistency of SWH measurements across different sensors. In particular, denoising is conducted using a non-parametric empirical mode decomposition (EMD) method to reduce random noise (Huang et al., 1998; Quilfen and Chapron, 2021), which effectively suppresses Gaussian noise while retaining small-scale variability in the data (Quilfen and Chapron, 2019, 2021).

Currently, the up-to-date publicly available version of the CCI-Sea State dataset is version 4 (v4). This dataset spans the period Aug 1991-Jan 2024. In previous versions, data of version 3 have gone through complete and consistent retracking of all included altimeters, ensuring greater uniformity across the dataset, whereas version 1 largely inherited the processing approaches from the GlobWave project and did not apply this level of consistency. Compared to versions 3, more satellites are included in v4, and SWH data from them have been more carefully re-edited and re-bias-corrected using altimeter tandem collocations, altimeter-buoy collocations, and altimeter cross-collocations in order to ensure better consistency between missions and instruments. This new altimeter dataset represents to date the longest continuous global wave climate data records. This dataset is now available at https://data-cersat.ifremer.fr/data/ocean-waves/cci-seastate/v4/, and a product user guide is available at https://cciseastate.gitlab-pages.ifremer.fr/ccidoc/intro.html.

2.1.2 WAVEWATCH III ST4 and ST6 Hindcasts

The SWH data from an NWM hindcast based on the WAVEWATCH III (WW3) source term package 6 (ST6) are used as the background field in this study. The WW3-ST6 configuration is based on the physical parameterizations of Liu et al. (2021), forced by ERA5 10-m surface winds (with a resolution of 0.25° × 0.25° × 1h). The model outputs are provided at 0.25° × 0.25° spatial resolution and 3 h temporal resolution. Without the assimilation of wave observations, the hindcast SWHs show good agreement with measurements, with an overall RMSE of ~0.35 m (5–15% of SWH) when compared with altimeter observations in the open ocean. Further details and access to the dataset are provided in Liu et al. (2021).

To assess the sensitivity of the results to the choice of background field, an additional NWM hindcast based on WW3 source term package 4 (ST4) is also used in this study. This dataset, known as the Integrated Ocean Waves for Geophysical and Other Applications hindcast, is based on the parameterizations of Ardhuin et al. (2010) and is forced by global 10-m

https://doi.org/10.5194/essd-2025-694
Preprint. Discussion started: 3 December 2025

wind fields from the Climate Forecast System Reanalysis (CFSR). The WW3-ST4 hindcast has also been shown to perform well against both buoy and altimeter observations of SWH (Rascle and Ardhuin, 2013), and it is publicly available via the IFREMER FTP server (ftp.ifremer.fr).

It is noted that a more recent version of WW3-ST6, forced by ERA5 winds, has been released and provides improved performance (Alday et al., 2023). However, in the present study our objective is to demonstrate that uncertainties in the background field have only a limited impact on the data fusion results. For this purpose, a dataset with more distinct differences from WW3-ST6 was required. Therefore, we use the earlier CFSR-forced WW3-ST4 hindcast as a contrasting background field.

2.1.4 CMEMS Gridded SWH Dataset

The gridded multi-mission merged satellite SWH data product from CMEMS is also used here to show that it is difficult to generate a good quality grided SWH data product by using only altimeter data. CMEMS multi-mission gridded SWH merges multiple along-track SWH data (Sentinel-6A, Jason-3, Sentinel-3A, Sentinel-3B, SARAL/AltiKa, Cryosat-2, CFOSAT, SWOT-nadir, HaiYang-2B and HaiYang-2C) and produces daily gridded data. Two SWH fields are produced including a 2° "daily mean" field computed from all available level 3 along-track measurements from 00:00 UTC until 23:59 UTC and a 0.5° "instantaneous" field at 12:00UTC using the same data source but accounting for their spatial and temporal proximity. However, after checking the data, it is found that the 2° "daily mean" field is not a "seamless" field with many grid points without data. Thus, only the "instantaneous" fields are used in this study. The data is available at https://doi.org/10.48670/moi-00180 (CMEMS 2024).

2.1.5 Buoy Observations

The 20-min averaged SWHs data obtained from the National Data Buoy Center (NDBC) are used as a reference in this study. We used observations from 50 NDBC buoys located more than 100 km offshore, covering the period 2010-2016, with buoy locations shown in Fig. 1. Although the NDBC data have undergone standard quality control, some spurious values remain; therefore, an additional screening was applied, retaining only records with 0.15 m < SWH < 15 m.

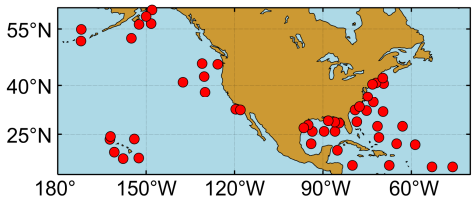

Fig.1. Locations of the 50 NDBC buoys used in this study.

https://doi.org/10.5194/essd-2025-694
Preprint. Discussion started: 3 December 2025

2.2 Fusion Methods

Prior to data fusion, a simple one-dimensional look-up table correction is applied to remove the systematic bias between SWHs from the WW3-ST6 hindcast data and the along-track altimeter observations. The data fusion method employed in this dataset is an improved yet relatively simple space-time optimal interpolation approach. This method is designed to maximize the retention of the original altimeter SWH observations within the fused product with the corresponding formula expressed as follow:

$$A(i,j,t) = M(i,j,t) + \sum_{k=1}^{N} w(i,j,t)_k \bullet (O_k - M_k) \quad (1)$$

$$w(i,j,t)_k = \exp\left[-d_k^2(i,j,t)/2R(i,j,t)^2\right] / \sum_{k=1}^{N} \exp\left[-d_k^2(i,j,t)/2R(i,j,t)^2\right] \quad (2)$$

$$R(i,j,t) = \min\left[d_k(i,j,t)\right] \quad (k = 1,2,3,...,N) \quad (3)$$

$$d_k(i,j,t) = C + \sqrt{(S_k/S_1)^2 + (T_k/T_1)^2 + Q\left[\left(M_k - M(i,j,t)\right)/M_k\right]^2} \quad \left(S_k < S_{thr} \;\&\; T_k < T_{thr} \;\&\; r_{i,j,k} > r_{thr}\right) \quad (4)$$

$$d_k(i,j,t) = +\infty \quad \left(S_k > S_{thr} \;or\; T_k > T_{thr} \;or\; r_{i,j,k} < r_{thr}\right)$$

where i, j, and t represent longitude, latitude, and time, respectively; M (model) and A (analysis) represent the NWM hindcast data before and after data fusion, respectively; $k \in \{1,2,...,N\}$ represents the number of altimeter observations; O_k and M_k represent the values of altimeter-observed and corresponding collocated modelled SWH at the k-th altimeter record; w_k represents the weight factor at spatio-temporal location (i, j, t) for the k-th altimeter record; d_k represent the distance from the model location (i, j, t) to the k-th altimeter record in a super-space spanned by space, time, and SWH, which is defined in Eq.(4); R represents the distance to the nearest altimeter record; C is a constant to mitigate the impact of cases with too small distance; S and T represent the spatial distance and the time difference between (i, j, t) and the k-th altimeter record, respectively, and S_1 and T_1 represent coefficients that make S and T dimensionless; Q is also a scaling coefficient that ensures the quantities of SWH, time, and space are comparable; $r_{i,j,k}$ is the correlation coefficient (CC) between the NWM-hindcast SWHs time series at grid location (i, j) and the time series at the location the k-th altimeter record within the corresponding month; S_{thr}, T_{thr}, and r_{thr} are threshold values for S_k, T_k, and $r_{i,j,k}$, respectively: An observation is excluded from consideration if either the space–time separation or the correlation between the model point and the observation point exceeds these thresholds.

To reduce potential space-time representativeness errors, all altimeter observations located within 75 km of coastlines were excluded, as SWH can vary substantially over short distances in nearshore regions due to bottom-wave interactions and coastal sheltering.

Here, C, S_1, T_1, Q, S_{thr}, T_{thr}, and r_{thr} are set to 8, 50 km, 90 min, 8000, 2000 km, 24 h, and 0.7, respectively, based on a straightforward but trivial tuning procedure which was conducted using the 2020 CCI-Sea State dataset. Specifically, Jason-2 data were withheld, and the remaining three altimeter missions (CryoSat-2, SARAL, and Sentinel-3A) were fused with the

https://doi.org/10.5194/essd-2025-694
Preprint. Discussion started: 3 December 2025

WW3-ST6 hindcast data. The fused results were then validated against the independent Jason-2 observations, and the parameter set yielding relatively smallest errors was selected. The error metrics considered in this evaluation include bias, RMSE, and correlation coefficient (CC):

$$Bias = \frac{1}{n}\sum_{i=1}^{n}(y_i - x_i) \quad (5)$$

$$RMSE = \sqrt{\frac{1}{n}\sum_{i=1}^{n}(y_i - x_i)^2} \quad (6)$$

$$CC = \sum_{i=1}^{n}(y_i - \bar{y})(x_i - \bar{x}) \Big/ \left[\sqrt{\sum_{i=1}^{n}(y_i - \bar{y})^2}\sqrt{\sum_{i=1}^{n}(x_i - \bar{x})^2}\right] \quad (7)$$

where x and y denote the SWH from two different datasets (in this case, fused dataset without Jason-1 and Jason-1 from CCI-Sea State) , respectively; n is the sample size, and the bars over them denote their mean values. It is worth noting that the results are not very sensitive to these tuning parameters near their optimal values. Varying these tuning parameters by −50 % to +100 % has only a negligible impact on the results, with changes in RMSE of less than 0.005 m and changes in CC of less than 0.003.

Compared to conventional optimal interpolation methods , which typically define weights solely based on the inverse squared spatial distance, our approach introduces several modifications to the distance definition to better reflect the characteristics of wave fields:

1) *Introduction of the temporal distance*. The distance definition incorporates the temporal separation between the model grid point to be corrected and the observation point. This accounts for the fact that the sea state at a given location is influenced not only by nearby observations in space but also by those in time. Consequently, both past and future observations are allowed to contribute to the correction at a given time, unlike most operational wave assimilation schemes, which generally exclude future data when updating past states.

2) *Introduction of SWH differences*. The difference in modelled SWH between the model grid point to be corrected and that with observation is also included. This modification addresses the anisotropic nature of storm-generated wave fields, particularly swell. Due to model arrival-time errors (Jiang et al., 2016), modeled wave fields may be spatially displaced relative to altimeter measurements. By assuming that “similar modelled SWHs within the same meterological event imply similar corrections”, this SWH-based distance partly accounts for anisotropy, giving relatively higher weight to observations within the same storm wave system compared to those outside. Experimental results demonstrate that including this term reduces RMSE by approximately 0.005 m.

3) *Introduction of a base distance C*. A constant base distance is included to mitigate cases where very small distances (approaching zero) would otherwise lead to unrealistically large weights. Without this adjustment, the fused results exhibit prominent along-track stripes corresponding to the altimeter ground tracks, which are physically implausible. During the tuning of C, visual inspection was first used to ensure the absence of such striping, followed by optimization to minimize RMSE.

https://doi.org/10.5194/essd-2025-694
Preprint. Discussion started: 3 December 2025

2.3 Two Types of Fused Data

During the data fusion process, the number of altimeter satellites used plays a critical role. In principle, assimilating more satellites increases the spatiotemporal coverage of the observations, which should, in turn, improve the accuracy of the fused dataset. However, as pointed out by Jiang (2020), the growing number of altimeters over time also increases the likelihood of sampling extreme events. This may introduce undersampling biases in long-term climate analyses. Although the fusion process can mitigate this issue to some extent, it may still remain a potential source of error in climate-related applications.

To address this concern, we adopt a strategy similar to that used in the Maps of Sea Level Anomalies product of AVISO, generating two complementary datasets: an *"all-sat" product*, which integrates observations from all available altimeter satellites in CCI-Sea State, and a *"two-sat" product*, which consistently fuses data from only two altimeters. The "all-sat" product prioritizes accuracy by maximizing data coverage, whereas the "two-sat" product emphasizes temporal consistency by maintaining a relatively fixed sampling pattern. From an application perspective, the "all-sat" product is better suited for tasks that demand higher accuracy, such as model evaluation and the training of deep learning algorithms. In contrast, the "two-sat" product is more appropriate for long-term climate analyses, where temporal consistency is of greater importance.

For the "two-sat" product, the selection of satellites is guided by sampling characteristics: one satellite with an orbit inclination of approximately 66° is paired with another in a near-polar orbit, in order to ensure a stable and consistent sampling pattern over time (Table 1). In cases where a given satellite experiences temporary data gaps, observations from another satellite with a similar orbital configuration are preferentially used as substitutes. For example, in the CCI-Sea State v3 dataset, Jason-2 data were missing during several days in June 2017 and March 2019. In such instances, Jason-3 data were used as replacements for Jason-2.

Table 1. Altimeters used in different periods for the "two-sat" product.

Time	1992/10-1995/5	1995/6 2002/1	2002/2-2008/7	2008/8-2010/6	2010/7-2016/2	2016/3-2023/12
Satellite1	TOPEX	TOPEX	JASON-1	JASON-2	JASON-2	JASON-3
Satellite2	ERS-1	ERS-2	ENVISAT	ENVISAT	CRYOSAT-2	CRYOSAT-2

3. Quality assessment of the Fused Dataset

3.1 Comparison against In-situ Data

The CMEMS gridded dataset, the WW3-ST6 dataset, and the fused dataset ("two-sat" version) were all bilinearly interpolated to each buoy location, and subsequently compared against the corresponding SWH of buoy observations. Figures 2a–c show scatter plots comparing buoy observations with the three datasets for instantaneous values at 12:00 UTC.

https://doi.org/10.5194/essd-2025-694
Preprint. Discussion started: 3 December 2025

Open Access Earth System Science Data Discussions

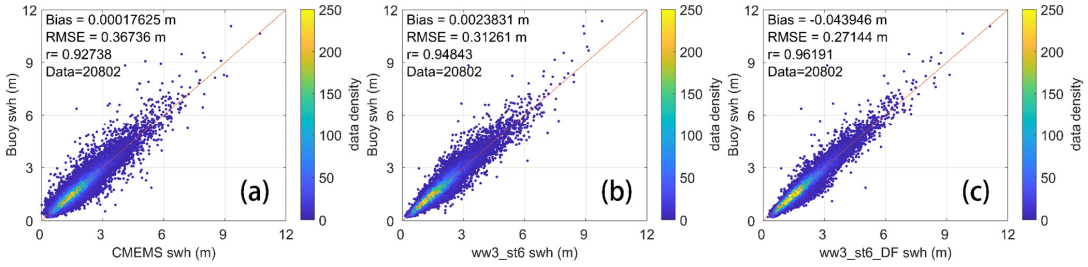

Fig. 2. Scatter plots comparing SWHs from buoy observations with those from (a) the CMEMS gridded dataset, (b) the WW3-ST6 dataset, and (c) the fused dataset ("two-sat" version) for instantaneous values at 12:00 UTC during the period 2010-2016. All gridded datasets were bilinearly interpolated to the buoy locations

The comparison of daily means between SWHs from the CMEMS gridded dataset and NDBC buoys (Fig. 2a) shows a bias of nearly zero, an RMSE of 0.37 m, and a CC of 0.93. Although these error metrics may not appear poor at first glance, they are substantially worse than the error metrics obtained from comparisons between along-track altimeter SWHs and buoys over the same period (e.g., Jiang, 2023). Moreover, they are significantly inferior to those from the NWM hindcast (WW3-ST6), which does not assimilate any observations (Fig. 2b, bias = 0.002 m, RMSE = 0.31 m, CC = 0.95). This finding supports our point raised in the Introduction Section that the accuracy of "independent" Level-4 gridded altimeter SWH products are often much lower than that of raw NWM outputs. However, after fusing WW3-ST6 with along-track altimeter observations, the RMSE further decreased to 0.27 m and the CC increased to 0.96, demonstrating the effectiveness of the data fusion approach.

3.2 Comparison against Altimeter Measurements

We further evaluated the global performance of the fused dataset using altimeter observations from 2011 to 2016. In this validation, one satellite was excluded from the fusion, while the remaining altimeter missions were fused with WW3-ST6. The excluded satellite was then used as an independent reference for evaluation. For example, in Fig. 3, Jason-2 was withheld and subsequently compared against the fused and unfused datasets.

Figure 3a shows the comparison between the original WW3-ST6 hindcast and Jason-2. The results indicate that even without assimilation, WW3-ST6 already achieves a relatively high accuracy, with a bias <0.1 m, an RMSE of 0.34 m, and a CC of 0.97. Figure 3b presents the outcome after applying a one-dimensional look-up table correction to WW3-ST6 SWHs using CCI-Sea State data prior to fusion. Although this calibration reduces the bias to a smaller value, its effect on RMSE and CC is negligible, with only a 0.01 m decrease in RMSE and a 0.001 increase in CC. This suggests that the pre-fusion correction was not the main contributor to accuracy improvement. In contrast, the fused dataset (Fig. 3c) shows substantial enhancement relative to Jason-2, with the bias remaining negligible, the RMSE reduced by nearly one third to 0.23 m, and the CC increased by more than 0.015 to 0.985, highlighting the high accuracy of the fused product.

https://doi.org/10.5194/essd-2025-694
Preprint. Discussion started: 3 December 2025

Open Access Earth System Science Data Discussions

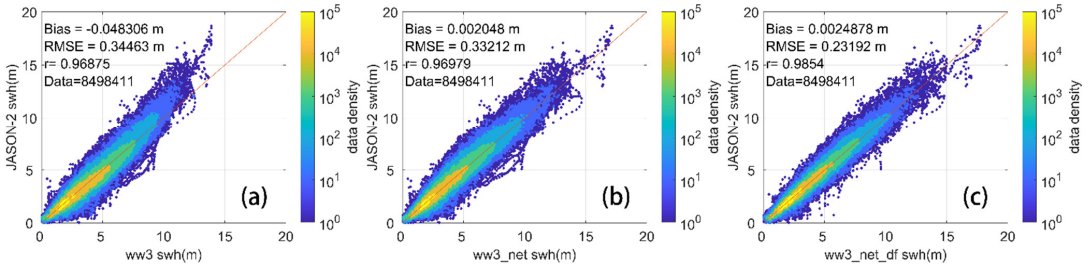

Fig. 3. Evaluation of the fused dataset using Jason-2 as an independent reference in 2011. (a) Comparison between the original WW3-ST6 hindcast and Jason-2. (b) Results after applying a one-dimensional look-up table correction to WW3-ST6 SWHs using CCI-Sea State data prior to fusion. (c) Comparison between the fused dataset (WW3-ST6 + remaining altimeters) and Jason-2. The fusion substantially reduces the RMSE and improves the correlation compared to both the original and bias-corrected hindcast.

Tables 2–4 summarize the evaluation results of bias, RMSE, and CC, respectively, for 2011. To reduce the volume of data processing, we restricted the analysis to the year 2011 only. In each experiment, two of the four available satellites were fused with WW3-ST6, while the remaining satellites were used as independent references. As shown in the tables, when any pair consisting of one satellite with a 66° inclination and one with a near-polar inclination was selected for fusion, all error metrics improved markedly compared with the original WW3-ST6 results. Specifically, the bias, which originally ranged from 0.03 to 0.06 m, was reduced to within 0.01 m. Such a small bias can be regarded as statistically negligible at the climate scale, which is meaningful for long-term climate analyses. Meanwhile, the RMSE decreased from 0.36–0.39 m to 0.23–0.25 m, representing a reduction of more than 30%, and the CC increased from about 0.95 to 0.98, also reflecting a substantial improvement. These results metrics consistently confirm the robustness and accuracy of the fusion dataset.

Table 2. Bias (in m) between WW3-ST6 and independent altimeter observations, as well as bias between the fused dataset and independent altimeter observations, in 2011. For each experiment, two satellites were selected for fusion with WW3-ST6, while the remaining satellites served as independent references.

Reference Mission	WW3-ST6	CRYOSAT-2 & JASON-1	CRYOSAT-2 & JASON-2	CRYOSAT-2 & ENVISAT	JASON-1 & JASON-2	JASON-1 & ENVISAT	JASON-2 & ENVISAT
CRYOSAT-2	-0.0354	—	—	—	0.0063	0.0062	-0.0001
JASON-1	-0.0675	—	-0.0123	-0.0143	—	—	-0.0113
JASON-2	-0.0590	0.0034	—	-0.0059	—	0.0024	—
ENVISAT	-0.0339	0.0072	0.0000	—	0.0083	—	—

Table 3. The same as Table 2, but for RMSE (in m).

Reference Mission	WW3-ST6	CRYOSAT-2 & JASON-1	CRYOSAT-2 & JASON-2	CRYOSAT-2 & ENVISAT	JASON-1 & JASON-2	JASON-1 & ENVISAT	JASON-2 & ENVISAT

https://doi.org/10.5194/essd-2025-694
Preprint. Discussion started: 3 December 2025

Open Access Earth System Science Data Discussions

CRYOSAT-2	0.3678	—	—	—	0.2336	0.2383	0.2404
JASON-1	0.3879	—	0.2504	0.2452	—	—	0.2443
JASON-2	0.3851	0.2498	—	0.2443	—	0.2434	—
ENVISAT	0.3733	0.2431	0.2418	—	0.2322	—	—

Table 4. The same as Table 2, but for CC.

Reference Mission	WW3-ST6	CRYOSAT-2 & JASON-1	CRYOSAT-2 & JASON-2	CRYOSAT-2 & ENVISAT	JASON-1 & JASON-2	JASON-1 & ENVISAT	JASON-2 & ENVISAT
CRYOSAT-2	0.9534	—	—	—	0.9811	0.9803	0.9800
JASON-1	0.9528	—	0.9796	0.9805	—	—	0.9806
JASON-2	0.9524	0.9793	—	0.9802	—	0.9803	—
ENVISAT	0.9545	0.9805	0.9806	—	0.9822	—	—

Comparison of the results in Tables 2–4 with those in Fig. 3 indicates that, when Jason-2 is used as the independent reference, the improvement in accuracy from fusing three satellites instead of two is marginal, with the RMSE reduced by only about 0.01 m and the CC increased by just 0.001. Similar results are obtained when other satellites are used as the reference, leading to the consistent conclusion that the additional reduction in errors is insignificant. This can be attributed to the fact that, after fusing two satellites, the overall accuracy of the fused dataset is already very close to the intrinsic accuracy of radar altimeter SWH measurements, which corresponds to a global RMSE of about 0.2 m according to previous studies (e.g., Ribl & Young, 2019; Jiang, 2020; Jiang, 2023). This further demonstrates the robustness of the fusion method.

Although these results suggest that adding more satellites beyond two does not substantially improve accuracy, we still generated an “all-sat” version of the dataset. This is because, despite the diminishing marginal benefits in terms of accuracy, additional satellites can still provide slight improvements. Moreover, the inclusion of more satellites may help to homogenize the spatial distribution of errors—reducing potential regional biases, especially in gaps between the ground tracks of the fused satellites. Importantly, as long as the altimeter observations themselves are more accurate than the background field (a condition met by all current missions), increasing the number of assimilated satellites will not degrade the overall accuracy.

Figure 4 shows the spatial distribution of errors corresponding to the data presented in Fig.3. The upper and lower panels respectively display the comparisons between the WW3-ST6 and Jason-2 SWH data before and after data fusion. The three columns represent the spatial distributions of bias, RMSE, and CC. Before fusion, the data exhibit opposite bias patterns between the high latitudes of the Northern and Southern Hemispheres, with the maximum bias reaching nearly 0.5 m. Such large biases also lead to RMSE values exceeding 0.5 m in high-latitude regions. Areas with low CC values are mainly concentrated in low-latitude regions, where the mean SWH is smaller and its annual variability is limited. In high-latitude regions, although the absolute errors are larger, the mean SWH and its variability are also higher, allowing the CC to remain above 0.9. After fusion, except for a few areas near sea ice, the bias is largely reduced to within ±0.1 m, the RMSE decreases to below 0.5 m, and the CC shows a clear improvement across both high- and low-latitude regions.

https://doi.org/10.5194/essd-2025-694
Preprint. Discussion started: 3 December 2025

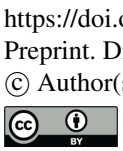

Open Access Earth System Science Data Discussions

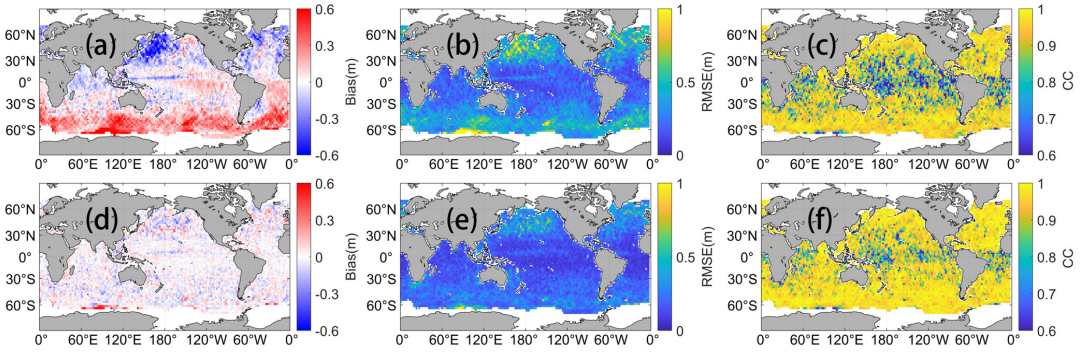

315 **Fig. 4.** Spatial distributions of SWH error metrics between WW3-ST6 and Jason-2 (a-c) before and (d-f) after fusing SWH data from CCI-Sea State: (a & d) bias, (b & e) RMSE, and (c & f) CC.

4. Discussion on the Importance of Background Fields

Section 3 has demonstrated the high accuracy of the fused dataset, which results from the complementary strengths of two components: (1) the relatively sparse but highly reliable altimeter observations, and (2) the less accurate yet 320 spatiotemporally "seamless" numerical wave hindcasts serving as the background field. Both components are indispensable. As shown previously, when no background field is used (which is equivalent to assuming a zero-valued background), the sparse altimeter observations alone cannot reconstruct a high-quality SWH field. This highlights the crucial role of the background field in ensuring the reliability and robustness of the fusion framework, but also suggests that the accuracy of the fusion product depends on the quality of the background field.

325 To assess the impact of background-field selection, we conducted fusion experiments for January 2011 using two different hindcasts: WW3-ST6 forced by ERA5 10-m winds and WW3-ST4 forced by CFSR 10-m winds. Figure 5 presents the results before and after data fusion. The first row (Figs. 5a–c) shows the direct comparison between the original WW3-ST6 and WW3-ST4 hindcasts in terms of bias, RMSE, and CC. Despite employing different parameterizations and wind forcing, both hindcasts were tuned against realistic SWH conditions and thus exhibit reasonable consistency. The bias 330 generally lies within ±0.3 m, RMSE remains below 0.6 m in most regions (though reaching ~0.8 m in parts of the westerlies and near-polar regions), and CC exceeds 0.9 in most regions with significant wave variability. Lower CC values (<0.8) appear around tropical swell pools (Chen et al., 2002; Jiang and Yang, 2022), mainly due to differences in source wind forcing and parameterizations that cause mismatches in swell arrival times (Jiang et al., 2016), combined with the inherently small SWH variability in these regions.

335 After fusion, the discrepancies between WW3-ST6 and WW3-ST4 are greatly reduced (Figs. 5d–f). With the exception of a few near-polar areas, the bias decreases to within ±0.05 m almost everywhere. RMSE also shows a widespread

https://doi.org/10.5194/essd-2025-694
Preprint. Discussion started: 3 December 2025

Open Access Earth System Science Data Discussions

reduction, with maximum values in the Northern Hemisphere westerlies not exceeding 0.4 m. CC is also markedly improved, exceeding 0.9 even within the "swell pools", substantially enhancing the consistency between the two datasets. The probability density functions of the three error metrics across all global grid points (Figs. 5g–i) further illustrate the improved agreement after fusion.

It is noted that the errors induced by different background fields are much smaller than the errors of monthly mean values introduced by undersampling when no background field is used. Therefore, although the fused product is not independent of the background field, which is as expected, the influence of the specific choice of background is not critical, provided that the background field offers a physically reasonable estimate of the large-scale SWH distribution. This also highlights the robustness of the proposed fusion approach across different model background fields. Moreover, the robustness with respect to the background further suggests that the altimeter observations are effectively assimilated into the fused dataset, making it well suited for applications such as the reconstruction and analysis of historical wave climate.

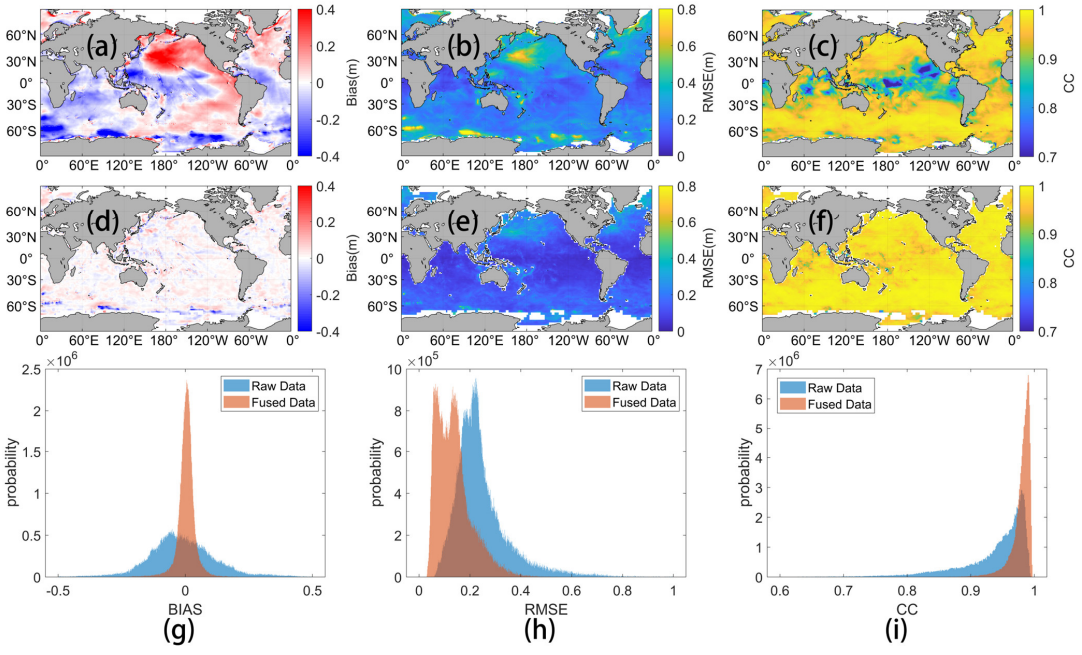

Fig. 5. Comparison between WW3-ST6 (forced by ERA5 winds) and WW3-ST4 (forced by CFSR winds) before and after data fusion in January 2011. (a–c) Maps of bias, RMSE, and CC between the two hindcasts before data fusion. (d–f) Same as (a–c), but after fusion with altimeter observations. (g–i) Probability density functions of grid-point bias, RMSE, and CC, respectively, illustrating the overall improvement in consistency between the two hindcasts after fusion.

https://doi.org/10.5194/essd-2025-694
Preprint. Discussion started: 3 December 2025

5. Applications of the Fused Dataset

5.1 Wave Climate Studies

One of the primary applications of the fused dataset is in wave climate studies. The fused product substantially reduces the undersampling errors that have long limited the use of altimeter data in wave climate analyses. Jiang (2020) showed that, when only two altimeter missions are available, undersampling can introduce an RMSE of approximately 0.17 m in the monthly mean SWH on a coarse 2° grid (assuming the altimeter SWH is error-free). While such errors may not strongly impact climatological means, they can still introduce additional uncertainty in trend estimates. More importantly, even on such a coarse 2° grid, the undersampling effect can still cause systematic underestimations exceeding 0.1 m in the monthly 90th percentile, with RMSEs larger than 0.4 m, and even greater biases at higher percentiles: the monthly 99th percentile may suffer from systematic underestimations over 0.7 m and RMSEs over 0.8 m. These biases decrease as the number of altimeter missions increases, but if not explicitly corrected (which may be a difficult task), they can lead to artificial trend errors far larger than the true climate signal. This suggests that previous studies on extreme wave climate based solely on along-track altimeter data (e.g., Izaguirre 2011; Partra et al. 2020; Takbash et al. 2019; Young and Ribal 2020) may be affected by such limitations, although the random error of altimeters may partially compensate for undersampling errors in extreme value analysis, which represents a topic worthy of further investigation in future work.

The fused dataset effectively mitigates these undersampling issues. In particular, it preserves the original resolution of the NWM in the open ocean, greatly reducing the need to account for grid-size effects on undersampling. Compared with the gridding of along-track data, the fused dataset also provides a more convenient and reliable basis for wave climate studies.

Figures 6a–d show the global mean SWH distribution for January 2011 derived from the original CCI-Sea State L4 data, the fused dataset, and their absolute and relative difference (with the fused dataset re-averaged to 1° resolution for the difference calculation). In Figure 6a, the distribution exhibits typical features of global wave fields in boreal winter, with high SWH in the Northern Hemisphere westerlies driven by extratropical storms. In comparison, the waves generated by the Southern Hemisphere westerlies are relatively smaller. During this month, the lowest mean SWH occurs in the region near the Arabian Sea in the Indian Ocean. In this month, the monsoon is inactive in this region and swells generated in the Southern Ocean cannot propagate into this area due to the blocking effects of the African continent and Madagascar. The original CCI–Sea State L4 data exhibit qualitatively consistent spatial patterns with the fused product (Fig. 6b). However, because of undersampling, the altimeter ground tracks remain clearly visible in the monthly mean fields of the CCI–Sea State L4 product. Figures 6c and 6d show the absolute and relative differences between Figs. 6a and 6b, respectively. In regions with large mean SWH, undersampling associated with satellite orbits can lead to biases approaching ±1 m. In regions with smaller mean SWH, although the absolute sampling error is typically within ±0.3 m, this seemingly small absolute error

https://doi.org/10.5194/essd-2025-694
Preprint. Discussion started: 3 December 2025

may still correspond to a relative error of up to 20%. Such undersampling errors can exert a significant influence on certain types of wave climate analyses.

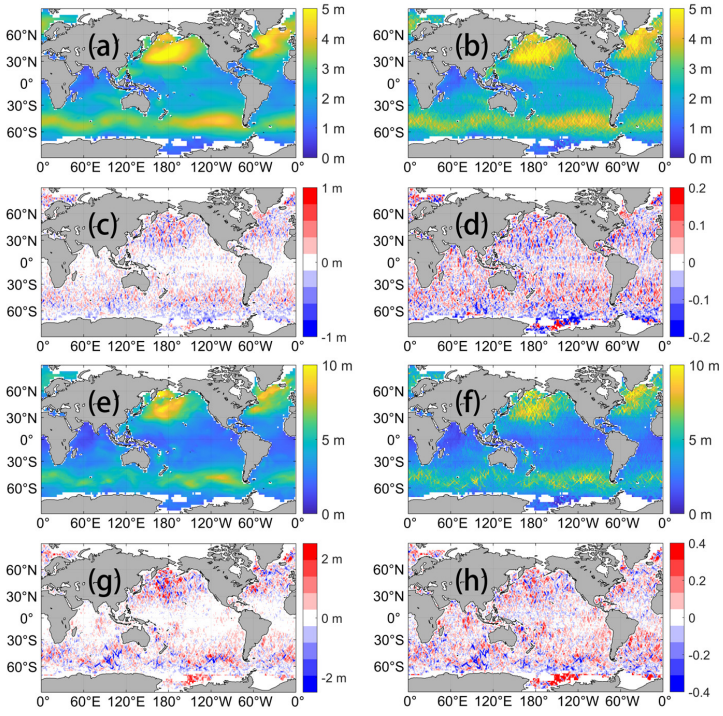

Figure 6. Global distributions of the monthly mean SWH in January 2011 derived from the (a) the fused dataset and (b) the original CCI-Sea State L4 dataset, as well as their (c) absolute difference and (d) relative difference. Panels (e–f) show the corresponding global distributions of the 95th-percentile SWH during the same period derived from (e) the fused dataset and (f) the original CCI-Sea State dataset, as well as their (g) absolute difference and (h) relative difference.

While the differences between the monthly mean SWH distributions in Figs. 6a and 6b are not particularly pronounced, Figs. 6e–h respectively present the global distribution of the 95th-percentile SWH in January 2011 derived from the original CCI-Sea State data at 1° resolution, the fused dataset, and their difference (with the fused dataset also re-averaged to 1° for comparison). The differences between Figures 6e and 6f are even more pronounced. When a storm is successfully captured by the altimeter, the 95th-percentile SWH derived from Fig. 6f is significantly higher than that in Fig. 6e. Conversely, if the altimeter fails to sample the waves generated by a storm (particularly the high SWH values during the storm), the 95th-

https://doi.org/10.5194/essd-2025-694
Preprint. Discussion started: 3 December 2025

400 percentile SWH in Fig. 6f becomes notably lower than that in Fig. 6e. This issue makes the orbital patterns and data discontinuities in Fig. 6f more apparent. Such undersampling can easily lead to errors exceeding 2 m (Fig. 6g) in the monthly 95th-percentile SWH and relative errors of over 40% (Fig. 6g).

It is worth noting that in January 2011, four altimeter satellites were operating simultaneously, which considerably reduced undersampling errors compared with periods when only two satellites were in orbit. Nevertheless, even under these 405 favourable conditions, such large errors still occur in the estimation of extreme wave heights, underscoring the necessity of data fusion.

A closer inspection further reveals that underestimation occurs more frequently than overestimation in the estimation of extreme SWH in Fig. 6f. This is because extreme wave events are generally less likely to be captured by the altimeter sampling, which has been pointed out by previous studies (Jiang, 2020). Jiang (2020) has further demonstrated that as the 410 number of satellites increases, the likelihood of such overestimation gradually diminishes, which may, in turn, affect the analysis of long-term climate trends.

Previous studies have also pointed out that the use of a 1° grid tends to underestimate altimeter-based SWH percentiles, and that coarser grids of 2° or 3° may be more appropriate (Young and Ribal, 2019; Takbash et al., 2019; Jiang, 2020). However, coarser grids inevitably lead to the loss of spatial detail. In addition, as the computation area increases, the 415 physical meaning of percentile estimates derived from altimeter observations becomes less clear: They will shift from the temporal percentiles of spatially averaged SWH within a given grid cell to the spatio-temporal percentiles of the broader region corresponding to the grid size. In contrast, percentiles computed from the fused dataset not only retain higher spatial resolution but also have a well-defined physical interpretation. For instance, when the 95^{th} or 99^{th} percentile is calculated at the native 0.5° resolution of the fused dataset, the resulting value corresponds directly to the extreme percentile of the time 420 series of spatially averaged SWH within each 0.5° grid cell.

5.2 Studies of AI Wave Model

In recent years, with the rapid development of artificial intelligence (AI), data-driven modeling approaches have re-emerged as a promising alternative to traditional numerical simulations. Compared with numerical models, AI-based methods offer lower computational cost and higher efficiency, and they have already achieved remarkable success in weather 425 forecasting. Large-scale AI models such as *Pangu*, *GraphCast*, *GenCast*, and *Aurora* have, in some cases, delivered forecasting skill surpassing that of numerical weather prediction (NWP) systems at a fraction of the computational expense. Similarly, we believe that AI-based wave models will represent a promising research direction in the future.

A key requirement for training high-performing AI models is the availability of large, accurate, and well-structured datasets. Although ERA5 SWH data already provide a reasonable source of training samples, as noted in Section 1, ERA5 430 does not incorporate future observations to constrain past states, leaving room for improvement. In one of our recent studies, we used a subset of the fused dataset in this study (limited to five years) to train and fine-tune an AI wave model for global SWH (Wang and Jiang 2024). Hindcast experiments demonstrated that the AI model fine-tuned with the fused dataset not

https://doi.org/10.5194/essd-2025-694
Preprint. Discussion started: 3 December 2025

only outperformed the counterpart trained directly on ERA5 but also significantly exceeded the hindcast skill of WW3-ST6. This indicates that the fused dataset enables AI wave models to achieve, in terms of SWH hindcast accuracy, performance that rivals or even surpasses state-of-the-art NWMs (Fig. 7).

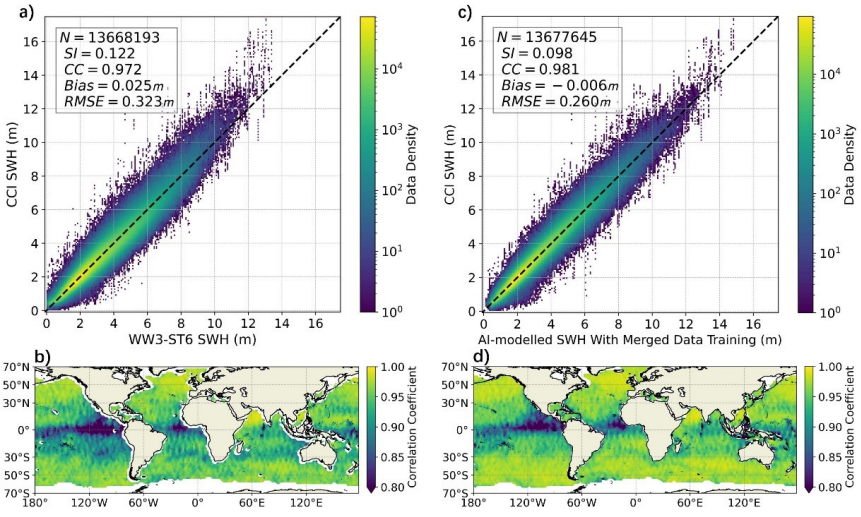

Fig. 7. Comparison between SWHs from numerical/AI wave models against CCI-sea state dataset for global ocean in 2020. (a) Scatter plot of SWHs from the NWM versus CCI-sea state. (b) Spatial distributions of CC between SWHs from NWM and CCI-sea state. (c, d) Same as (a, b), respectively, but for the AI wave model trained with ERA5 and subsequently fine-tuned using the 5-year fused dataset. Note that the year 2020 is excluded from the model training.

More details of this AI wave model and how this fused dataset is used can be found in Wang and Jiang (2024). Meanwhile, it is noted that we additionally provide the *R* value in Eq. 3, which represents the spatiotemporal distance to the nearest altimeter observation, to further adapt the fused dataset for AI training applications. Intuitively, a smaller *R* value indicates stronger influence from altimeter measurements, which allow it to be incorporated into the training loss function as a weight, so that data points closer to direct observations can be assigned higher importance. This *R* value and corresponding weighting strategy was also employed in Wang and Jiang (2024).

6. Data Description and Availability

The fused data is freely available at https://doi.org/10.57760/sciencedb.29314 (Su and Jiang, 2025). Two versions are provided: (1) a *two-sat* version, which incorporates data from only two altimeters at any given time and is primarily intended for wave climate studies; and (2) a *multi-sat* version, which integrates observations from as many concurrent altimeter

https://doi.org/10.5194/essd-2025-694
Preprint. Discussion started: 3 December 2025

missions as possible and is designed to support applications such as the training of artificial intelligence-based wave models. The data are stored in standard NetCDF grid format, with SWH and the distance parameter *R* expressed as functions of latitude, longitude, and time. Each NetCDF file corresponds to one calendar month, with global attributes documenting metadata such as the source WW3-ST6 hindcast file, the names of the fused satellites, the start and end time, the identifiers of the fused satellites, and the percentage contribution of each satellite dataset to the fusion.

7. Summary

Satellite altimeters can provide long-term, high-accuracy observations of SWH across the global ocean. However, their inherently sparse spatial and temporal coverage introduces undersampling errors, which can limit the reliability of wave climate analyses, particularly for extreme wave climate. To address this limitation, we employ WW3-ST6 hindcast outputs as a background field and perform an offline fusion with along-track, jointly calibrated altimeter observations from the CCI Sea State dataset. Validation against buoy measurements and independent satellite data demonstrates that the resulting fused gridded product achieves high accuracy. To cater to different applications, two versions of the fused dataset are provided: (1) a *two-sat* version, which incorporates data from only two satellites at any given time and is optimized for wave climate studies, ensuring temporal consistency throughout the record; and (2) a *all-sat* version, which assimilates observations from as many altimeter missions as possible and is intended for applications such as training artificial intelligence-based wave models, where high spatial and temporal fidelity is critical.

Although such a high-accuracy gridded dataset offers many practical advantages, it also has some limitations compared with Level-2 altimeter observations due to the interpolation involved. For instance, it is not well suited for studying regional-scale variations in the SWH spectrum, because many high-frequency signals in the Level-2 observations are filtered to adapt to the model resolution. In addition, because the background field used in the fusion does not account for wave–current interactions, the fused dataset is not appropriate for studies focusing on such interactions, even though some signals of wave–current interaction may be present in the original altimeter observations.

The fused dataset is generated based on the inter-calibrated altimeter dataset from the CCI-Sea State. Although altimeter inter-calibration can largely mitigate systematic biases between different missions, as noted by Dodet et al. (2021), there remain substantial uncertainties in the long-term climate calibration of altimeter SWH due to limitations in the calibration methods and reference in situ data. In addition, with improvements in instrument precision and online data processing over time, the observational uncertainties (random errors) of both altimeters and buoys have generally decreased (Jiang, 2023). Inter-calibration cannot eliminate differences in observational uncertainty and random error among different satellites, which may introduce minor errors in extreme value analyses and warrants further investigation, although these random errors are largely reduced by spatiotemporal averaging during the fusion.

Despite these limitations, this fused dataset can already provide substantial utility in many applications. Moreover, considering the advantages of a gridded product over along-track observations, there are clear avenues for future

https://doi.org/10.5194/essd-2025-694
Preprint. Discussion started: 3 December 2025

enhancement. Despite these limitations, this fused dataset already offers substantial utility across a wide range of applications. One of the simplest and most direct ways to further enhance the dataset is to increase both the number of fused observations and the temporal coverage. The current dataset is based solely on satellites included in the CCI-Sea State dataset, while data from some more recent missions such as Haiyang-2 and CFOSAT have not yet been incorporated. Incorporating these post-2020 altimeter and wave-scatterometer observations would not only enable a more reliable "all-sat" fusion product, but also, by extending the analysis period, allow relatively weak climate signals, particularly long-term trends, to emerge more clearly.

Author contributions

Conceptualization: HJ
Methodology: HS
Investigation: HS, HJ
Visualization: HS
Supervision: HJ
Writing—original draft: HJ, HS
Writing—review & editing: HJ

Competing interests

All authors declare that they have no competing interests.

Acknowledgments

This work was jointly supported by the National Key Research and Development Program of China (2023YFC3008203) and the National Natural Science Foundation of China (42376172).

Code and data availability

The CCI sea state product is available at https://data-cersat.ifremer.fr/data/ocean-waves/cci-seastate/v4/. WAVEWATCH III ST4 and ST6 Hindcasts are available from Rascle and Ardhuin (2013) and Liu et al. (2021), respectively. The gridded multi-mission merged satellite SWH data product from CMEMS is from https://doi.org/10.48670/moi-00180 (CMEMS 2024). The NDBC buoy data are available from https://www.ndbc.noaa.gov/. The fused dataset is available at https://doi.org/10.57760/sciencedb.29314 (Su and Jiang 2025). The AI wave model is available from Wang and Jiang (2024).

https://doi.org/10.5194/essd-2025-694
Preprint. Discussion started: 3 December 2025

Reference

Alday, M., Accensi, M., Ardhuin, F., and Dodet, G.: A global wave parameter database for geophysical applications. Part 3: Improved forcing and spectral resolution, *Ocean Modell.*, 166, 101848, doi:10.1016/j.ocemod.2021.101848, 2021.

Ardhuin, F., Rogers, E., Babanin, A. V., Filipot, J.-F., Magne, R., Roland, A., van der Westhuysen, A., Queffeulou, P., Lefevre, J.-M., Aouf, L., and Collard, F.: Semiempirical dissipation source functions for wind-wave models: part I, definition, calibration and validation, *J. Phys. Oceanogr.*, 40, 1917–1941, doi:10.1175/2010JPO4324.1, 2010.

CMEMS (Copernicus Marine Service Information), Global Ocean L 4 Significant Wave Height From Nrt Satellite Measurements, Marine Data Store [dataset], doi: 10.48670/moi-00180, 2024.

Chen, G., Chapron, B., Ezraty, R., and Vandemark, D.: A global view of swell and wind sea climate in the ocean by satellite altimeter and scatterometer, *J. Atmos. Oceanic Technol.*, 19, 1849-1859, doi:10.1175/1520-0426(2002)019<1849:AGVOSA>2.0.CO;2, 2002.

Dodet, G., Piolle, J.-F., Quilfen, Y., Abdalla, S., Accensi, M., Ardhuin, F., Ash, E., Bidlot, J.-R., Gommenginger, C., Marechal, G., Passaro, M., Quartly, G., Stopa, J., Timmermans, B., Young, I., Cipollini, P., and Donlon, C.: The Sea State CCI dataset v1: towards a sea state climate data record based on satellite observations, *Earth Syst. Sci. Data*, 12, 1929–1951, doi:10.5194/essd-12-1929-2020, 2020.

Fan, Y., Lin, S., Held, I. M., Yu, Z., and Tolman, H. L.: Global ocean surface wave simulation using a coupled atmosphere-wave model, *J. Clim.*, 25, 6233-6252, doi:10.1175/JCLI-D-11-00621.1, 2012.

Fan, Y., Held, I. M., Lin, S., and Wang, X.: Ocean warming effect on surface gravity wave climate change for the end of the 21st century, *J. Climate*, 26, 6046-6066, doi:10.1175/JCLI-D-12-00410.1, 2013.

Fan, Y., Lin, S., Griffies, S. M., and Hemer, M. A.: Simulated Global Swell and Wind Sea Climate and Their responses to Anthropogenic Climate Change at the End of the 21st Century, *J. Clim.*, 27, 3516-3536, doi:10.1175/JCLI-D-13-00198.1, 2014.

Huang, N. E., Shen, Z., Long, S. R., Wu, M. C., Shih, H. H., Zheng, Q., Yen, N.-C., Tung, C. C., and Liu, H. H.: The empirical mode decomposition and the Hilbert spectrum for nonlinear and non-stationary time series analysis, *Proc. Roy. Soc. A-Math. Phy.*, 454, 903–995, doi:10.1098/rspa.1998.0193, 1998.

Hersbach, H., Bell, B., Berrisford, P., Hirahara, S., Horányi, A., Muñoz-Sabater, J., Nicolas, J., Peubey, C., Radu, R., Schepers, D., Simmons, A., Soci, C., Abdalla, S., Abellan, X., Balsamo, G., Bechtold, P., Biavati, G., Bidlot, J., Bonavita, M., De Chiara, G., Dahlgren, P., Dee, D., Diamantakis, M., Dragani, R., Flemming, J., Forbes, R., Fuentes, M., Geer, A., Haimberger, L., Healy, S., Hogan, R. J., Hólm, E., Janisková, M., Keeley, S., Laloyaux, P., Lopez, P., Lupu, C., Radnoti, G., De Rosnay, P., Rozum, I., Vamborg, F., Villaume, S., and Thépaut, J.-N.: The ERA5 global reanalysis, Q. *J. Roy. Meteor. Soc.*, 146, 1999–2049, doi:10.1002/qj.3803, 2020.

Izaguirre, C., Méndez, F. J., Menéndez, M., and Losada, I. J.: Global extreme wave height variability based on satellite data, *Geophys. Res. Lett.*, 38, L10607, doi:10.1029/2011GL047302, 2011.

https://doi.org/10.5194/essd-2025-694
Preprint. Discussion started: 3 December 2025

Jiang, H. and Yang, Z.: A revisit of global wind-sea and swell climate and variability using multiplatform altimeters, *Remote Sens. Environ.*, 271, 112922, doi:10.1016/j.rse.2022.112922, 2022.

Jiang, H.: Evaluation of altimeter undersampling in estimating global wind and wave climate using virtual observation, *Remote Sens. Environ.*, 245, 111840, doi:10.1016/j.rse.2020.111840, 2020.

Jiang, H.: Random, Environmental, and Representativeness Errors in Ocean Remote Sensing Versus In Situ Data: An Example of Wave Heights From Altimeters, *IEEE Trans. Geosci. Remote Sens.*, 61, 1–13, doi:10.1109/TGRS.2023.3285348, 2023.

Jiang, H., Babanin, A. V., and Chen, G.: Event-based validation of swell arrival time, *J. Phys. Oceanogr.*, 46, 3563–3569, doi:10.1175/JPO-D-16-0208.1, 2016.

Liu, Q., Babanin, A. V., Rogers, W. E., Zieger, S., Young, I. R., Bidlot, J.-R., and Durrant, T. H.: Global wave hindcasts using the observation-based source terms: Description and validation, *J. Adv. Model. Earth Sys.*, 13, e2021MS002493, doi:10.1029/2021MS002493, 2021.

Meucci, A., Young, I. R., and Breivik, Ø.: Wind and Wave Extremes from Atmosphere and Wave Model Ensembles, *J. Climate*, 31, 8819–8842, doi:10.1175/JCLI-D-18-0217.1, 2018.

Patra, A., Min, S.-K., and Seong, M.-G.: Climate variability impacts on global extreme wave heights: Seasonal assessment using satellite data and ERA5 reanalysis, *J. Geophys. Res.-Oceans*, 125, e2020JC016754, doi:10.1029/2020JC016754, 2020.

Quilfen,Y. and Chapron, B.: On denoising satellite altimeter measurements for high-resolution geophysical signal analysis, *Adv. Space Res.*, 68, 875–891, doi:10.1016/j.asr.2020.01.005, 2021.

Quilfen, Y. and Chapron, B.: Ocean surface wave-current signatures from satellite altimeter measurements, *Geophys. Res. Lett.*, 46, 253–261, doi:10.1029/2018GL081029, 2019.

Rascle, N. and Ardhuin, F.: A global wave parameter database for geophysical applications. Part 2: Model validation with improved source term parameterization, *Ocean Modell.*, 70, 174-188, doi:10.1016/j.ocemod.2012.12.001, 2013.

Ribal, A. and Young, I. R.: 33 years of globally calibrated wave height and wind speed data based on altimeter observations, *Sci. Data*, 6, 77, doi:10.1038/s41597-019-0083-9, 2019.

Semedo, A., Sušelj, K., Rutgersson, A., and Sterl, A.: A global view on the wind sea and swell climate and variability from ERA-40, *J. Clim.*, 24, 1461-1479, doi:10.1175/2010JCLI3718.1, 2011.

Semedo, A., Vettor, R., Breivik, Ø., Sterl, A., Reistad, M., Soares, C. G., and Lima, D.: The wind sea and swell waves climate in the Nordic seas, *Ocean Dynam.*, 65, 223-240, doi:10.1007/s10236-014-0788-4 , 2015.

Semedo, A., Weisse, R., Behrens, A., Sterl, A., Bengtsson, L., and Günther, H.: Projection of global wave climate change towards the end of the Twenty-First Century, *J. Climate*, 26, 8269-8288, doi:10.1175/JCLI-D-12-00658.1, 2013.

Sterl, A. and Caires, S.: Climatology, variability and extrema of ocean waves: The web-based KNMI/ERA-40 wave atlas, *Int. J. Climatol.*, 25, 963–977, doi:10.1002/joc.1175, 2005.

https://doi.org/10.5194/essd-2025-694
Preprint. Discussion started: 3 December 2025

580 Stopa, J. E. and Cheung, K. F.: Periodicity and patterns of ocean wind and wave climate, *J. Geophys. Res.-Oceans*, 119, 5563–5584, doi:10.1002/2013JC009729, 2014.

Su, H. and Jiang, H.: Significant wave height fusing multi-mission altimetry and WW3 hindcast, V3. Science Data Bank, , doi:10.57760/sciencedb.29314, 2025.

Takbash, A., Young, I. R., and Breivik, Ø.: Global Wind Speed and Wave Height Extremes Derived from Long-Duration
585 Satellite Records, *J. Climate*, 32, 109–126, doi:10.1175/JCLI-D-18-0520.1, 2019.

Timmermans, B. W., Gommenginger, C. P., Dodet, G., and Bidlot, J.-R.: Global wave height trends and variability from new multi-mission satellite altimeter products, reanalyses and wave buoys, *Geophys. Res. Lett.*, 47, e2019GL086880, doi:10.1029/2019GL086880, 2020.

Wang, X. and Jiang, H.: Physics-guided deep learning for skillful wind-wave modeling, *Sci. Adv.*, 10, eadr3559,
590 doi:10.1126/sciadv.adr3559, 2024.

Young, I. R. and Ribal, A.: Multiplatform evaluation of global trends in wind speed and wave height, *Science*, 364, eaav9527, doi:10.1126/science.aav9527, 2020.

Zieger, S., Vinoth, J., and Young, I. R.: Joint calibration of multiplatform altimeter measurements of wind speed and wave height over the past 20 years, *J. Atmos. Ocean. Technol.*, 26, 2549–2564, doi:10.1175/2009JTECHA1303.1, 2009.